Original Article

Development of an Osteogenic Scaffold Via Combination of Natural and Synthetic Polymers for an Enhanced Cell-Compatible Nano-Network

Elnaz Rostami, Solmaz Rostami, Alireza Bonakdar, Simzar Hosseinzadeh, Hassan Rajabi Maham

DOI: 10.34172/PS.026.43186

To appear in: Pharmaceutical Science (https://ps.tbzmed.ac.ir/)

Received date: 17 Sep 2025

Revised date: 28 Dec 2025

Accepted date: 4 Jan 2026

Please cite this article as: Rostami E, Rostami S, Bonakdar A, Hosseinzadeh S, Rajabi Maham H. Development of an osteogenic scaffold via combination of natural and synthetic polymers for an enhanced cell-compatible nano-network. Pharm Sci. 2026. doi: 10.34172/PS.026.43186

Development of an osteogenic scaffold via combination of natural and synthetic polymers for an enhanced cell-compatible nano-network

Elnaz Rostami[1], Solmaz Rostami[2], Alireza Bonakdar[3], Simzar Hosseinzadeh[4*], Hassan Rajabi Maham[1*]

[1]Department of Animal Sciences and Biotechnology, Faculty of Life Sciences and Biotechnology, Shahid Beheshti University, 1983963411, Tehran, Iran

[2]Department of Animal Biology, School of Biology, University College of Science, University of Tehran, 141556455, Tehran, Iran

[3]Department of Tissue Engineering and Applied Cell Sciences, School of Advanced Technologies in Medicine, Shahid Beheshti University of Medical Sciences, 1968917313, Tehran, Iran

[4]Medical Nanotechnology and Tissue Engineering Research Center, Shahid Beheshti University of Medical Sciences, 1968917313, Tehran, Iran

Co-corresponding authors:

*Dr. Simzar Hosseinzadeh, s.hosseinzadeh@sbmu.ac.ir ORCID ID: 0000-0001-8749-2447

*Dr. Hassan Rajabi-Maham, h_rajabi@sbu.ac.ir

Abstract

Background: Nanoscale scaffolds play a significant role in bone tissue engineering due to their appropriate biological activity which can be enhanced by the incorporation of nanoparticles such as graphene oxide (GO). This study aimed to develop a growth factor-free scaffold based on polyurethane (PU), cellulose acetate (CA) and GO nanoparticles for bone regeneration using electrospinning technique.

Methods: Here, the scaffolds composed of PU, PU-CA and PU-CA-GO, were fabricated to assess the bone differentiation of human adipose-derived mesenchymal stem cells (MSCs). The scaffolds were characterized and after cell culture, the biological assessments such as

Alizarin Red staining (ARS), alkaline phosphatase (ALP) activity and calcium mapping were employed to evaluate the osteogenic differentiation of MSCs.

Results: Scanning electron microscopy (SEM) results demonstrated that GO nanoparticles were successfully dispersed within the PU-CA polymer matrix any agglomerations. The fiber diameters of PU-CA and PU-CA-GO scaffolds were 1500±400 and 1250±320 nm. Plasma-treated PU-CA-based scaffolds exhibited hydrophilic surfaces with water contact angles of 19° and 0° for PU-CA and PU-CA-GO scaffolds after 10s, respectively. Moreover, the incorporation of GO increased the Young's modulus of the scaffolds from 1290 to 1380 kPa and the strain from 8.54 to 9.37 %. In addition, osteogenic differentiation as assessed by ARS staining, ALP activity and calcium deposition, indicated that PU-CA-GO scaffold provided a suitable matrix for the osteogenic differentiation of MSCs after 21 days. The ARS values for the scaffolds without and with GO nanosheets were 14.41±0.7% and 32.88±1.1%, respectively. Furthermore, the ALP levels for both scaffold types were 8±1 and 17±2.5 IU/mg. Accordingly, calcium deposition was 1.03 W% Ca for the GO-free control group and 1.23 W% Ca for the GO-containing scaffold.

Conclusion: In general, this scaffold could be considered a promising growth factor-free candidate for bone tissue engineering. However, further *in vivo* evaluations are recommended in future studies.

Keywords: Cellulose acetate; Polyurethane; Graphene oxide; Osteogenic differentiation; Mesenchymal stem cell; growth factor-free

Introduction

Recently, individual over the age of 50 in developed countries have increasingly suffered from musculoskeletal diseases. Based on relevant investigations, bone tissue injuries can lead to trauma, infection, tumors and local disorders.[1] Numerous challenges such as site morbidity, limited suitability for large bone grafts and discomfort at the injury site, are associated with conventional methods of bone tissue engineering, including repairing surgery, autotransplantation and allotransplantation.[2] The World Health Organization (WHO) designated 2000 to 2010 as the golden era for development of bone defect regeneration worldwide. Accordingly, tissue engineering has been considered an interdisciplinary field that integrates knowledge from chemistry, physics, engineering, biology and medicine to address musculoskeletal disorders.[3] It has been demonstrated that transplantation of mesenchymal stem cells (MSCs) into diabetic patients can control glycemia and preserve beta-cells were preserved.[4] In another clinical study, patients with diabetic foot ulcers (DFU) experienced wound size reduction following MSC transplantation.[5] MSCs also elicited a therapeutic response in patients with amyotrophic lateral sclerosis (ALS).[6] Moreover, in the context of viral infections such as SARS-CoV-2, MSCs have been shown to exert beneficial effects by modulating immune system activity.[7] Among MSCs sources, adipose tissue has been most frequently utilized due to its availability and the ease with which its isolated cells differentiate.[8] These cells possess a high capacity for tissue repair and regeneration. Adipose tissue is considered a favorable source of MSCs due to the relative abundance of MSCs, their multipotency and the simplicity of cell harvest. As highly active primary cells, MSCs can differentiate into various lineages including adipocytes, osteoblasts and chondrocytes.[9] Their self-renewal capacity also increases the number of cells available for *in vitro* research.[10] In a clinical study on patients with spinal cord injury (SCI), MSCs caused no side effects and led to improvement in motor function.[11] Additionally, this cell source was employed to treat mandible fractures. Patients treated with MSCs showed 36.48% higher ossification rate compared to the control group receiving only fracture reduction.[12] Furthermore, 13 patients with cranio-maxillofacial skeleton defects were treated with adipose-derived MSCs cultured in β-tricalcium phosphate. The results showed 10 of these patients had successful outcomes.[13] Therefore,

although bone marrow-derived MSCs possess greater osteogenic potential, their limited presence as 0.001%–0.1%, makes adipose tissue a more practical cell source.[14] However, it has been noted that this strategy should be companied with osteoconductive materials to effectively promote bone formation.[15] Table 1 summarizes current clinical trials involving the application of MSCs in treating various disease treatments. The use of nanofibers as a scaffold mimics the structure of the extracellular matrix (ECM). Electrospinning with its ability to generate micro- and nanoscale polymeric fibers, has gained significant attention in tissue engineering. It is considered an easy, scalable, versatile and cost-effective method for producing fibers of various diameters, ranging from nanometers to several micrometers, in different forms.[16] Recently, electrospinning nanofibers have been applied as effective matrices in bone regeneration and repair studies.[17] These scaffolds, which support bone cell growth, can improve mechanical strength, serve as structural support for cell proliferation, exhibit ECM-like morphology and aid in maintaining the phenotype of cultured cells.[18] Beyond the structure of the scaffold, the choice of material significantly influences cell behavior. Cellulose acetate (CA) is a synthetic polymer derived from the esterification of cellulose with acetic acid.[19] The acetate ester of cellulose offers several advantages, including biodegradability, compatibility with hydroxyl-containing substances, biocompatibility and adequate flexural and tensile strength. These features encourage its use in nanofiber mat fabrication.[20] CA is widely employed in bone ingrowth applications due to its hydrophilicity, biodegradability and ability to support mineralization. Overall, CA has shown significant potential in tissue engineering by promoting osteogenic differentiation and osteoblast proliferation.[21] However, due to its high modulus, low breaking stress, limited resistance to strain, CA is typically used as a component in composite materials. Thus, it is unsuitable on its own for biomedical load-bearing applications.[22]

Polyurethane (PU) is another widely used polymers in tissue engineering and has been combined with CA to improve mechanical properties. Depending on the raw materials used, PU is a biocompatible, biodegradable and non-toxic polymer with high tensile strength that contributes to better resistance. PU is composed from three main components: 1) the polyol, 2) the chain extender and 3) the diisocyanate. Polyol provides a soft segment with hydroxyl (-OH) groups, the chain extender contains small molecules with amine or hydroxyl groups and diisocyanate is a low molecular weight compound that reacts with both.[٢٣] PU can be

formulated into a wide range of mechanical properties and chemical structures, resulting in coatings, foams, films, fibers and fibers for bone regeneration applications.[24] Many researchers have reported PU as a key material in bone tissue engineering. However, its hydrophobic nature limits its ability to support cell proliferation and adhesion.[٢٥] Hence, combining CA and PU can mitigate the limitations of both polymers. To further enhance mechanical strength, researchers have incorporated graphene derivatives into scaffolds. In addition to improving physical characteristics, graphene derivatives promote cell differentiation and proliferation due to their great biocompatibility at controlled concentrations. Graphene also modulates the scaffold surface to support cell differentiation, enhancing osteoblast adhesion, proliferation and growth.[26] Graphene oxide (GO), a form of graphite with angstrom-scale thickness, contains oxygen-containing functional groups at the edges (Carbonyl and Carboxyl) and on the surface (hydroxyl and epoxide). Owing to its unique chemical, physical and mechanical properties-as well as excellent biocompatibility, GO represents a promising material for bone regeneration.[27] By stimulating the differentiation of bone-like stem cells, this nanoparticle holds great potential for bone tissue engineering applications.[28]

As a whole, the establishment of a scaffold with intrinsic differentiation-inducing properties, without the need for exogenous growth factors or reparative agents, is a key priority in scaffold design. This strategy creates a regenerative microenvironment free from external bioactive compounds that may lead to unpredictable side effects. Moreover, the translation of *in vitro* and *in vivo* findings into clinical trials and regulatory approval processes, becomes more straightforward and safer when growth factors and drugs are avoided. Previous studies have supported this concept. For example, a fully interconnected hollow channel network with an aligned nanopatterned surface (HCAS) provided a cell- and biological factor–free approach for vascularization and bone regeneration.[29] In another study, a nanofibrous scaffold functionalized with M2 macrophage–derived exosomes enabled angiogenesis and osteogenesis without the addition of cells or growth factors.[30] A scaffold composed of poly(lactic-co-glycolic acid) (PLGA) and poly(γ-ethyl-L-glutamate) (PELG) did not fully match the mechanical properties of native osteochondral tissue, however, its high porosity and intrinsic bioactivity promoted chondrogenic differentiation of mesenchymal stem cells without the use of conditioned media.[31] Additionally, composite materials based

on poly (L-lactic acid), poly(ε-caprolactone), poly (3-hydroxybutyrate-co-3-hydroxyvalerate) and Sr-doped nanohydroxyapatite demonstrated a balanced regulation of osteogenesis and osteoclastogenesis in co-cultures of human bone marrow mesenchymal stem cells and human peripheral blood mononuclear cells. Notably, this regenerative response occurred in the absence of growth factors or conditioned media. Also, the results approved that this scaffold beside mechanical stimulation induced M2 macrophage polarization.[32] Similarly, a cell- and factor-free scaffold network composed of polycaprolactone, hydroxyapatite and calcium peroxide exhibited appropriate mechanical strength and enabled controlled oxygen release, thereby supporting angiogenic activity and bone repair.[33]

This research introduces a novel growth factor–free scaffold capable of providing a favorable hydrophilic microenvironment for efficient cell attachment, adequate mechanical strength and intrinsic osteoinductive potential. The synergistic combination of PU, CA and GO was strategically employed to support the proliferation and osteogenic differentiation of human adipose-derived MSCs without the need for exogenous bioactive factors. By relying on the physicochemical and structural properties of the scaffold, this approach enhances safety, cost-effectiveness and translational feasibility. The graphical abstract schematically illustrates the overall design concept and key outcomes of the present study.

Materials and Methods

Chemicals and reagents

All materials were of analytical (laboratory) grade and used as received without further purification. The materials used for the synthesis of graphene oxide (GO) nanoparticles, including potassium permanganate ($KMnO_4$) and sodium nitrate ($NaNO_3$), were purchased from Sigma-Aldrich (USA). Hydrogen peroxide (H_2O_2) was obtained from Merck. The polymers including polyurethane (PU, Mw of 80,000 -120,000 g/mol) and cellulose acetate (CA, Mw of 30,000 g/mol) were also supplied by Sigma-Aldrich (USA). Solvents such as tetrahydrofuran (THF), N,N-dimethylformamide (DMF), ethanol, acetic acid and dimethyl sulfoxide (DMSO) were purchased from Merck (Germany). Biological materials, including phosphate-buffered saline (PBS, pH≈7.5), Dulbecco's modified Eagle's medium (DMEM) and fetal bovine serum (FBS), were obtained from Gibco (Grand Island, NY, USA). Collagenase

type I used for cell isolation was purchased from Sigma-Aldrich (USA), and 3-(4,5-dimethylthiazol-2-yl)-2,5-diphenyl tetrazolium bromide (MTT), used for cell viability assessment, was obtained from Sigma (Germany). For cell nucleus staining, 4',6-diamidino-2-phenylindole (DAPI) was purchased from Sigma-Aldrich (UK). Glutaraldehyde used for cellular fixation was supplied by Sigma-Aldrich (USA). The reagent used for the biocompatibility assay, 3-(4,5-dimethylthiazol-2-yl)-2,5-diphenyltetrazolium bromide (MTT), was obtained from Sigma (Germany). For osteogenic characterization, Alizarin Red S (ARS) staining was purchased from Sigma (USA) and the alkaline phosphatase (ALP) assay kit was obtained from Parsazmon (Iran).

Synthesis and Characterization of GO

The modified Hummer's method was employed to synthesize GO nanoparticles.[34] Initially, 23 ml of 98% sulfuric acid was mixed with 0.5 g of graphite powder, followed by the gradual addition of 3 g of KMnO4 and 0.5 g of NaNO3. The mixture was then stirred at the relative centrifugal force (RCF) of 715 × g for 4 hours at 36°C. Subsequently, 3 ml of 30 wt.% H_2O_2 and 40 ml of deionized water were added to the solution. To remove impurities, the solution was washed for at least 3 times with deionized water. The byproducts of the chemical reactions are water-soluble and were therefore easily removed during the washing process. The resulting laminated GO nanosheets were then subjected to sonication (100 kHz, 120 W, for 30 minutes[35]) using an ultrasonic bath (YA XUN YX-2100, China) and collected via centrifugation at the RCF of 17888 × g, for 20 minutes. Finally, transmission electron microscopy (TEM) (JEOL, JEM-2000EXII) was employed to analyze the morphological characteristics of the GO nanoparticles.

Preparation of polymer and GO solutions

A 6 wt.% PU solution was prepared by dissolving PU in the 1:3 volume ratio of THF to DMF. The mixture was stirred at the RCF of 100 × g for 14 hours at room temperature (RT) to obtain a homogenous solution. For the fabrication of the PU-CA scaffold, a CA solution (18 wt.%) was prepared by dissolving cellulose acetate in 3:1 ratio of deionized water to acetic acid. Then, the CA and PU solution were combined in a 1:3 volume ratio. To prepare the PU-

CA-GO nanocomposite, 0.001 g of the GO was dispersed in THF via stirring for 1 hour and then added to the mixed PU-CA solution. Finally, the three prepared solutions were loaded into syringes and processed using an electrospinning device (Nanoazma, Iran).

Fabrication of nanofibrous scaffolds by electrospinning technique

The solutions were transferred to individual syringes and processed using an electrospinning device at a distance of 19 cm under electric field of 15 kV. The drum speed and flow rate were set to 300 rpm and 0.2 µl/hour respectively. All solutions were electrospun for 7 hours and the resulting fibers were collected on the drum. To enhance the surface hydrophilicity of the scaffolds, they were treated in a plasma generator (Diener Electronics, Germany) for 3 minutes. Finally, for cell seeding, the fabricated scaffolds were rinsed with PBS and sterilized with 70% ethanol under UV radiation for 20 minutes. The sterilized scaffolds were then immersed in DMEM containing 10% FBS and incubated at 37°C to assess potential microbial contamination.

Characterization of nanofibrous nanofibers by SEM, FTIR, water contact angle and tensile

Scanning electron microscopy (SEM, Philips XL30; Philips, Netherlands) was used to examine the morphology, structure and fiber diameter distribution of the nanofibers. Prior to imaging, the scaffold specimens were gold-coated and analyzed under an accelerating voltage of 25 kV. ImageJ software (National Institute of Health, USA) was employed to measure the fiber diameters from the SEM images.

The water contact angle (Krüss, Hamburg, Germany) was measured to evaluate the hydrophilicity of the scaffolds, both with and without plasma treatment. Scaffolds were cut into 1×1 cm^2 pieces and 2 µl of the deionized water was dropped onto the surface. Images were captured after 0, 5 and 10 seconds using Data Physics instrument (GmbH, Germany) to determine the contact angle.

Fourier transform infrared spectroscopy (FTIR, ALPHA FTIR Spectrometer, Bruker, Germany) was performed to identify functional groups present in the scaffolds, with spectra recorded over the wavenumber range of 4000-400 cm^{-1}.

The mechanical properties of the scaffolds were assessed using a tensile test performed on an Instron Universal Testing Machine (Model STM-20, SANTAM, Iran) with a load cell of 50 N. The scaffolds were cut into strips (0.5 × 3 cm^2), mounted on a paper frame and subjected to tension until their failure. Finally, strain at break, elastic modulus, ultimate tensile strength and stress-strain curves were obtained and compared among the scaffold groups.

Cells culture and characterizations by SEM and DAPI

Samples of adipose tissues were collected through abdominoplasty under the ethical approval number of IR.SBMU.REC.1401.026 from Shahid Beheshti University of Medical sciences, Tehran, Iran. After multiple washes, 0.1% collagenase type I was added to enzymatically digest the tissue. The enzyme activity was neutralized after 2 hours by adding culture medium containing FBS. The digested tissue was then centrifuged at the RCF of 4472 × g for 4 minutes and the isolated cells were cultured in DMEM supplemented with 10% FBS at 37◦C in a 5% CO2 incubator. These cells were characterized using flow cytometry technique, as described in our previous studies and the results are provided in Supplementary file 1.[36,37] Following cell seeding onto the scaffolds, the presence of cells was confirmed by DAPI staining. For this analysis, scaffolds were seeded with 1 × 10^4 cells per well and DAPI staining was performed on days 1, 14 and 21 days. The culture medium was removed and the specimens were washed with PBS and incubated with 4% glutaraldehyde for 40 minutes. The wells were then washed 3 times with PBS and stored in dark and cold conditions until imaging using fluorescent microscopy (Nikon Instruments, USA). Cell attachment to the scaffolds was also assessed using SEM on days 14 and 21. For SEM preparation, the cell-seeded scaffolds were washed with PBS, fixed in 4% glutaraldehyde for 2 hours and dehydrated using a graded ethanol series (50%, 60%, 70%, 80%, 90% and 100%). Finally, the samples were sputter-coated with gold and examined under SEM.

Cell viability and adhesion by MTT

The biocompatibility of the scaffolds was evaluated using MTT assay. The experimental groups included PU, PU-CA and PU-CA-GO scaffolds and the assessment was performed on days 1, 3, 7 and 14 after cell seeding. A tissue culture polystyrene (TCPS) surface was used as the control group, following the same protocol. In this assay, the culture medium was removed from each well and the samples were washed with PBS. Then, MTT solution (10% v/v in culture medium) was added to each group and incubated for 3.5 hours at 37° C. After the incubation, DMSO was added to dissolve the formazan crystals formed by viable cells. The absorbance of each sample including the scaffold groups and TCPS, was measured using a microplate reader (BioTek, USA) at 570 nm. The cell viability (%) was calculated using the following formula:[38]

Cell viability (%) = Average absorption of control sample / Average absorption of test samples × 100

Additionally, this assay can be adapted to assess cell attachment through a slight modification. Therefore, 4 hours after cell seeding on the scaffolds, the scaffolds were transferred to new wells. The samples were then washed with PBS and the MTT solution was added. After an incubation period of 3.5 hours, the absorbance values were measured at 570 nm. The optical density (OD) values were converted to cell numbers by using the MSC doubling time standard curve.

Mineral production by ARS

ARS was used to confirm the mineralized matrix developed on days 14 and 21 after cell seeding. To perform this, the cell-cultured scaffolds were rinsed with PBS and fixed with 4% glutaraldehyde for 40 minutes. Then, 100 µl of Alizarin Red was added to each specimen and incubated for 20 minutes at RT, followed by washing with PBS. Next, the samples were photographed suing an Olympus BX46 microscopy (Japan). The results were analyzed using ImageJ software to quantify the surface area of mineralized regions.

Quantification of Alkaline phosphatase synthesis by ALP assay

ALP enzyme plays a crucial role in mineralization during the osteogenic signaling pathway. To measure ALP activity, 600 µl of RIPA buffer was added to lyse cells after 7, 14 and 21 days of the cell seeding. The scaffolds were then transferred to microtubes, water-bath sonicated for 2 minutes and centrifuged at the RCF of 160992 × g at 4 °C for 5 minutes. The supernatants containing total proteins were resulted and 50 µL of this supernatant was mixed with 50 µL of ALP substrate solution (p-nitrophenyl phosphate). The sample was incubated at 37° C for 90 minutes and ALP activity was measured using a microplate reader (BioTek, USA) at 405 nm. The absorbance values of the groups were normalized against total protein content and ALP activity was reported as IU/mg of total protein.

Calcium deposition by EDS

The calcium content of the scaffolds after cell culturing for 21 days, was evaluated to detect differentiation of the seeded MSCs using energy-dispersive X-ray spectroscopy (EDS). This technique generates compositional maps of the specimens. For SEM images, the scaffolds on days 7 and 14 were washed with PBS, fixed by 4% glutaraldehyde for 2 hours, dehydrated using a serial dilution of ethanol and then examined by EDS.

Statistical analysis

This study presents the data as means ± standard deviation (SD). Two-way ANOVA and t-test were employed to compare the means between multiple groups and two groups, respectively (Graph Pad Prism 4.0, San Diego, California USA).

Results

TEM and SEM of GO and nanofibers

The morphology of GO synthesized by the modified Hummer's method was investigated using TEM image. The results show that the synthesized GO nanoparticles are layered and

wrinkled (Figure 1A). Moreover, SEM images reveal the fibers are regular, uniform and bead-free. Based on the findings, the average diameter of the PU (Figure 1Ba, d), PU-CA (Figure 1Bb, e) and PU-CA-GO (Figure 1Bc, f) nanofibers of scaffolds were 1100 ± 310, 1500 ± 400 and 1250 ± 320 nm, respectively.

Water contact angles of scaffolds

The wettability properties of the scaffolds were evaluated via water contact angle measurements. The corresponding values of PU, PU-CA and PU-CA-GO scaffolds prior to the plasma treatment were 94◦, 62◦ and 60◦, respectively. These values changed after the plasma treatment to 92◦, 33◦ and 50◦, respectively (Figure 2).

Chemical functional groups of scaffolds

To characterize the chemical groups of polymers and nanoparticles, FTIR spectra of the PU, PU-CA and PU-CA-GO samples were evaluated (Figure 3). The spectroscopy of the PU sample demonstrated the characteristic peaks at 600 to 620 cm^{-1} corresponding to the benzene rings in PU and the peaks at 1057, 1597 and 1459 cm^{-1} represent ester, carbonyl and amine groups, respectively.[39] The adsorption peaks of the CA polymer were detected at 1743 and 1235 cm^{-1}, corresponding to its hydroxyl and ether groups.[40] Additionally, the bands at 1072 and 1622 cm^{-1} are derived from the epoxide groups and C–C bonds of the GO nanoparticles.[34]

Mechanical properties of scaffolds

The mechanical attributes, such as strain at break, Young's modulus and ultimate tensile strength, were assessed by plotting the stress-strain curve of the scaffolds in Figure 4. Table 2 shows the results of the tensile strength test of the electrospun scaffolds. The PU scaffold had a higher strain value (230%) compared to other groups. However, the presence of GO nanoparticles with the polymers in the PU-CA-GO scaffold, increased the strain and ultimate

tensile strength compared to the PU-CA group, while there was no remarkable difference in Young's modulus between them.

Morphology and presence of cells on scaffolds

As shown in Figure 5, cell morphology and interactions with the nanofibers indicate that the cells were well adhered after 14 and 21 days. On days 1, 14 and 21, the scaffolds were stained with DAPI to confirm the presence of MSCs cells on them (Figure 6). The cell nucleus was approved on all scaffold groups and the increasing number of the cells during the culture period indicated the biocompatibility of the scaffolds, as well as the results from the MTT assay. However, some cell colonies were observed, especially with the PU-CA and PU-CA-GO scaffolds. It should be noted that the difference between the cell population across the different scaffolds was relatively similar.

Cell viability and attachment of scaffolds

The MTT assay was conducted after 1, 3, 7 and 14 days to evaluate the growth and proliferation of MSCs on TCPS, PU, PU-CA and PU-CA-GO scaffolds. The cell viability values confirmed that all scaffold groups showed an increasing trend over time. The PU-CA-GO scaffold exhibited the highest cell activity after 14 days of cell seeding (Figure 7a). The number of active cells after 1 day in the TCPS group was higher compared to the other groups, particularly the PU scaffold ($P \leq 0.05$). On day 14, the PU-based scaffolds showed significant differences from the control group (TCPS) (****$P \leq 0.001$, ***$P \leq 0.01$, ** $P \leq 0.05$). According to the results, the scaffolds showed higher cell viability, except after 1 and 3 days. These data confirm the mitotic effect of the scaffolds on MSCs [41], as evidenced by the gradual increase in cell number from 1 to 14 days. Moreover, to evaluate cell attachment, the MSCs cells were seeded on the scaffolds and after 4 hours, the MTT assay was performed. The results shown in Figure 7b, illustrated that the cell adhesion was lower in all scaffold groups compared to TCPS. However, the PU-CA-GO scaffold exhibited values closer to the control group, confirming better attachment condition with this scaffold when compared to the other scaffold groups. This outcome may be related to the surface

properties influenced by the presence of GO. Specifically, these nanoparticles increase the roughness of the scaffold surface, thereby enhancing cell attachment.[42]

Mineral deposition of scaffolds

To demonstrate mineral deposition as an osteogenic marker, ARS staining was performed after 14 and 21 days. As clearly shown in Figure 8, mineral deposits were observed on PU-CA and PU-CA-GO scaffolds at both time points, with the amount increasing over time. According to Figure 8, more mineral deposits were formed in the GO-containing scaffold (13.51% after 14 days), as marked by arrows and this value further increased after 21 days to 32.88%. This result is consistent with other studies that confirm the osteogenic potential of GO nanoparticles.[43] Statistically significant differences among the groups are presented in Figure 9a, with clear distinctions observed between all groups at both time points.

ALP activity of scaffolds

The synthesis of the osteogenic factor, ALP, was measured and presented in Figure 9b after 7, 14 and 21 days. As an early marker of osteogenesis [44], ALP activity exhibited the highest levels on day 7, followed by a decrease at the subsequent time points. The GO-containing scaffold showed the highest ALP activity compared to the other groups (*** $P \leq 0.01$).

Ca mapping of scaffolds

The EDS results indicated that the PU-CA-GO scaffold had higher calcium deposition than the other nanofibrous scaffolds (W% of Ca; 1.23), although the difference was not pronounced when compared to the PU-CA scaffold (W% of Ca; 1.03). In contrast, the PU scaffold showed a substantially lower calcium content (W% of Ca; 0.33) in Figure 10. In this assay, calcium minerals illustrated peaks corresponding to Ca Lα, CaKα and CaKβ ions in the scaffolds, with varying intensities between the groups.

Discussion

Growth factor–free and drug-free scaffolds that rely on their intrinsic structure and material composition are a priority for guiding tissue regeneration. This approach emphasizes simplicity, safety and translational feasibility from experimental studies to clinical applications. In addition, such scaffolds can be fabricated at low cost and avoid the potential side effects associated with bioactive molecule delivery. Therefore, positioning the scaffold as a growth factor–free and drug-free platform represents a key innovative aspect of this study. For decades, the challenge has been to develop a material with complete biodegradation within a predetermined time frame. Among polymers, polysaccharides such as CA are well-known due to their abundant and inexpensive sources [45], as well as their acetyl-groups, which contribute to a more resistant compound to degradation.[۴۶] However, due to the low mechanical strength and stability of CA, the use of these polymers has been limited. Therefore, new strategies have been developed to combine CA with the other polymers known for their superior mechanical properties and long-lasting durability. In this study, CA was chosen for its biological effects on wound healing [47] and its simple degradation mechanism via hydrolysis by endoglucanases (EGs) from microorganisms.[48] To enhance the durability of the final scaffold, CA was electrospun with PU. Additionally, the antibacterial properties of cellulose acetate provided another advantage, although this aspect was not explored in this study. Another important feature of CA is its ability to support cell bioactivity without requiring surface treatments.[49] This characteristic is crucial for promoting cell adhesion, which in turn can facilitate tissue regeneration.

In this study, a scaffold was fabricated by combining PU, CA and GO nanoparticles via electrospinning. The scaffold's features, including cell interaction, proliferation and differentiation, were assessed in the presence of MSCs, along with the physical and chemical characterizations of the scaffold. The electrospinning technique provided conditions similar to the natural ECM in terms of fiber scale, which is conductive to MSC differentiation.

Recently, various types of nanoparticles have been incorporated into tissue engineering to improve both the mechanical and biological properties of scaffolds. The inclusion of these nanoparticles opens new avenues for tissue repair.[50] GO nanoparticles, in particular,

promote bone differentiation of progenitor cells, thereby aiding in bone regeneration. In this study, this nanoparticle was successfully synthesized using the modified Hummer technique, yielding a wrinkled and lamellar structure. This wrinkled surface enhances their consistency, facilitates proper interactions with other polymers and improves their distribution within the polymer matrix.[36,51]

Prior to the cell viability test, the properties of PU, PU-CA and PU-CA-GO scaffolds were investigated. According to SEM images used to analyze the nanofibers, the morphology of electrospun fibers was nanoscale and homogeneous in all groups [52], indicating that a uniform environment was provided for the cells across the entire surface. According to the results, GO nanoparticles increased the electrical conductivity of the PU-CA solution and therefore, the fiber diameter decreased from 1500 ± 400 to 1250 ± 320 nm. The results of the water contact angle analysis showed that the scaffolds were initially in the hydrophobic range before the plasma treatment. However, after the plasma treatment, they shifted to the hydrophilic range. Also, the incorporation of CA and GO nanoparticles into PU, demonstrated that hydrophilic functional groups, including oxygen- and hydrogen-containing bonds, increased the surface polarity, thereby enhancing hydrophilicity. These hydrophilic nanofibers promote greater cell adhesion and proliferation compared to hydrophobic nanofibers. Moreover, enhanced hydrophilicity facilitates the uniform distribution of cells across the scaffold surface. Based on the results, PU had more hydrophobic behavior than the PU-CA and PU-CA-GO scaffolds. Therefore, owing to the possibility of hydrogen bonding and the presence of hydrophilic functional groups such as oxygen-containing moieties, the scaffolds containing CA and GO nanoparticles demonstrated increased hydrophilicity.[26] Similarly, Aidun *et al*. showed that the addition of GO nanoparticles to polycaprolactone/chitosan/collagen scaffolds significantly increased the surface hydrophilicity.[53] FTIR analysis confirmed the presence of characteristic chemical bands corresponding to the material used in each scaffold. The distinctive functional groups of CA and PU polymers were identified and the signature peaks of GO nanoparticles were also observed, verifying their successful incorporation. Due to the critical influence of mechanical properties on cell fate processes such as proliferation, migration, spreading and differentiation [54], this characteristic was examined using the tensile testing method. The PU, PU-CA and PU-CA-GO scaffolds exhibited Young's modulus of 1024, 1290 and 1380 kPa,

respectively. Consistent with previous findings, the increase in this parameter plays a crucial role in cell differentiation.[55] Based on these results, incorporation of CA and GO increased the ultimate tensile strength of the scaffolds, while the presence of GO nanoparticles reduced the elongation value of the composite scaffold. The observations from the MTT assay confirmed that all scaffolds; particularly the PU-CA-GO nanocomposite, had suitable biocompatibility and were non-toxic to MSCs, as indicated by other reports.[56-58] Thus, GO appears to enhance the biocompatibility and bioactivity of scaffolds toward MSCs. Additionally, the cell viability results could be attributed to the higher hydrophilicity of the scaffold.[59] SEM findings confirmed that MSCs were able to attach to all scaffold groups. Based on previous studies, it was expected that hydrophilic polymers and GO nanoparticles could facilitate cell attachment. In this regard, Fu *et al*. showed that the proliferation and attachment of E1-MC3T3 cells on the Gel-PLGA-GO nanofibrous scaffold were significantly higher than on the pure PLGA nanofiber scaffold. In particular, the incorporation of GO nanofiber into Gel-PLGA scaffolds increased ALP activity and calcium deposition in E1-MC3T3 cells.[56] The osteogenic differentiation of MSCs on PU, PU-CA and PU-CA-GO scaffolds was evaluated by assessing calcium deposition through ARS staining, measuring ALP activity and conducting EDS analysis. ALP is an enzyme that indicates cellular mineralization during bone differentiation by activating signaling pathways in progenitor cells. Significant differences in calcium deposition and ALP activity were observed in the PU-CA-GO scaffold compared to the other scaffold groups at all-time points. Therefore, GO-containing scaffold can be considered a promising candidate for promoting bone differentiation.

These data were further confirmed by Alizarin Red staining, quantification of mineralization degree and calcium mapping. On days 14 and 21, the ALP results were consistent with those obtained from Alizarin Red staining. Elkhenany *et al*. also investigated bone differentiation using tricalcium phosphate (TCP) and GO nanoparticles. They reported that these nanoparticles could enhance the osteogenic differentiation of MSCs isolated from bone marrow after 21 days *in vitro*. Since the ARS showed a significant amount of calcium in the differentiated cells, they demonstrated that GO as a non-toxic and biomimetic nanomaterial, could promote the formation of mineralized tissue.[60] In this context, Fu *et al*. indicated that GO functions as an osteogenic factor by triggering mineralization.[56]

Furthermore, it has been confirmed that when MSCs are incubated within an appropriate osteogenic scaffold, mineralization of that scaffold inevitably occurs.[61]

This study demonstrates several important advantages in the design of a growth factor–free scaffold for bone tissue engineering. The electrospun PU–CA–GO scaffold successfully promoted osteogenic differentiation of human adipose-derived MSCs through its intrinsic structural, physicochemical and mechanical properties, without the addition of exogenous growth factors. The homogeneous dispersion of graphene oxide within the polymer matrix enhanced scaffold hydrophilicity and mechanical performance, which in turn supported cell attachment, proliferation and osteogenic maturation, as confirmed by *in vitro* assays, including ALP activity, Alizarin Red staining and calcium deposition. The use of human MSCs and a characterization approach further strengthen the translational relevance of the findings. However, despite these promising results, the study is limited to *in vitro* evaluations and a relatively short culture period, which restricts conclusions regarding long-term performance, biodegradation behavior and *in vivo* bone regeneration capacity. In addition, the mechanical properties of the scaffold were not directly compared with those of native bone tissue and the effects of different graphene oxide concentrations were not explored. Furthermore, angiogenic potential and long-term cytotoxicity associated with graphene oxide were not assessed. Therefore, while the PU–CA–GO scaffold shows strong potential as a growth factor–free platform for bone tissue engineering, further *in vivo* studies and long-term evaluations are necessary to confirm its clinical applicability.

Conclusion

This study was one of the first *in vitro* studies on the bone differentiation of MSCs using a biocompatible, mechanical resistant and osteogenic scaffold composed of GO nanoparticles, PU and CA without the need for external growth or differentiating factors. As CA increased hydrophilicity of the PU-based scaffold, GO nanoparticles enhanced both mechanical and osteogenic potential. Therefore, this study offers new insights into the design of scaffolds with high structural and functional resemblance to bone tissue and its ECM. Accordingly, this scaffold may be proposed as a promising candidate for bone reconstruction and repair

applications without the use of any growth biomolecules. Although, the incorporation of GO nanoparticles showed encouraging results in promoting bone differentiation, further investigations, including the evaluation of additional parameters and *in vivo* studies, are necessary.

Authors' Contribution

Conceptualization: Simzar Hosseinzadeh

Investigation: Elnaz Rostami, Solmaz Rostami

Supervision: Simzar Hosseinzadeh, Hassan Rajabi Maham

Writing–original draft: Elnaz Rostami

Writing–review & editing: Alireza Bonakdar, Simzar Hosseinzadeh, Hassan Rajabi Maham

Competing Interests

The authors declare no conflict of interest.

Ethical Approval

This study was done under ethical code of IR.SBMU.REC.1401.026 from Medical Nanotechnology and Tissue Engineering Research Center of Shahid Beheshti University of medical sciences, Tehran, Iran.

Funding

This study was supported by a grant (ID: 43002437) from Medical Nanotechnology and Tissue Engineering Research Center of Shahid Beheshti University of medical sciences, Tehran, Iran.

References

1. Migliorini F, La Padula G, Torsiello E, Spiezia F, Oliva F, Maffulli N. Strategies for large bone defect reconstruction after trauma, infections or tumour excision: A comprehensive review of the literature. Eur. J. Med. Res. 2021;26 .١١٨:(١)

2. Singhal I, Tartaglia GM, Panda S, Herguner Siso S, Inchingolo AM, Del Fabbro M, et al. Tooth allografts as natural biocomposite bone grafts: Can they revolutionize regenerative dentistry? J. Compos. Sci. 2025;9(10):550 .

3. Karimi Z, Seyedjafari E, Mahdavi FS, Hashemi SM, Khojasteh A, Kazemi B, et al. Baghdadite nanoparticle-coated poly l-lactic acid (plla) ceramics scaffold improved osteogenic differentiation of adipose tissue-derived mesenchymal stem cells. J. Biomed. Mater. Res. A 2019;107(6):1284-93 .

4. Zhang W, Ling Q, Wang B, Wang K, Pang J, Lu J, et al. Comparison of therapeutic effects of mesenchymal stem cells from umbilical cord and bone marrow in the treatment of type 1 diabetes. Stem cell res. ther. 2022;13(1):406 .

5. Zhang C, Huang L, Wang X, Zhou X, Zhang X, Li L, et al. Topical and intravenous administration of human umbilical cord mesenchymal stem cells in patients with diabetic foot ulcer and peripheral arterial disease: A phase i pilot study with a 3-year follow-up. Stem cell res. ther. 2022;13(1):451 .

6. Siwek T, Jezierska-Woźniak K, Maksymowicz S, Barczewska M, Sowa M, Badowska W, et al. Repeat administration of bone marrow-derived mesenchymal stem cells for treatment of amyotrophic lateral sclerosis. Med. Sci. Monit. 2020;26:e927484-1 .

7. Eiro N, Cabrera JR, Fraile M, Costa L, Vizoso FJ. The coronavirus pandemic (sars-cov-2): New problems demand new solutions, the alternative of mesenchymal (stem) stromal cells. Front. cell dev. biol. 2020;8:645 .

8. Mazini L, Rochette L, Amine M, Malka G. Regenerative capacity of adipose derived stem cells (adscs), comparison with mesenchymal stem cells (mscs). Int. J. Mol. Sci. 2019;20(10):2523 .

9. Xu L, Liu Y, Sun Y, Wang B, Xiong Y, Lin W, et al. Tissue source determines the differentiation potentials of mesenchymal stem cells: A comparative study of human mesenchymal stem cells from bone marrow and adipose tissue. Stem cell res. ther. 2017;8:1-11 .

10. Li N, Wu Q. Foxm1 maintains homeostasis and self-renewal in wharton's jelly mesenchymal stem cells. Genes 2025;16(12):1517 .

11. Tahmasebi F, Barati S. Effects of mesenchymal stem cell transplantation on spinal cord injury patients. Cell Tissue Res. 2022;389(3):373-84 .

12. Castillo-Cardiel G, López-Echaury AC, Saucedo-Ortiz JA, Fuentes-Orozco C, Michel-Espinoza LR, Irusteta-Jiménez L, et al .Bone regeneration in mandibular fractures after the application of autologous mesenchymal stem cells, a randomized clinical trial. Dent. Traumatol. 2017;33(1):38-44 .

13. Gu C, Tang Q, Li L, Chen Y. Optimization and implication of adipose-derived stem cells in craniofacial bone regeneration and repair. Bioeng. 2024;11(11):1100 .

14. Im GI. Bone marrow-derived stem/stromal cells and adipose tissue-derived stem/stromal cells: Their comparative efficacies and synergistic effects. J. Biomed. Mater. Res. A 2017;105(9):2640-8 .

15. Tiberio F, Amato F, Desiderio C, Vincenzoni F, Perini G, Moretti I, et al. The osteoconductive properties of graphene-based material surfaces are finely tuned by the conditioning layer and surface chemistry. Mater. Adv. 2024;5(11):4772-85 .

16. Keirouz A, Wang Z, Reddy VS, Nagy ZK, Vass P, Buzgo M, et al. The history of electrospinning: Past, present and future developments. Adv. Mater. Technol. 2023;8(11):2201723 .

17. Khorshidi S ,Solouk A, Mazinani S, Mirzadeh H. A review on different approaches for improving cell infiltration in electrospun nanofibrous scaffolds. Pathobiol. Res 2016;18(4):1-22 .

18. Ortega Z, Alemán ME, Donate R. Nanofibers and microfibers for osteochondral tissue engineering. Osteochondral tissue engineering: Springer; 2018. p. 97-123.

19. Porpora F, Dei L, Forcellini C, D'Aleo C, Lisi L, De Sanctis M, et al. Interactions between polyethyleneimine xerogels and acetic acid vapor from degraded cellulose acetate. A novel therapy for motion picture films affected by the “vinegar syndrome”. Macromol. Rapid Commun. 2025:2500075 .

20. Alprol AE. Physicochemical characterization of nanocellulose: Composite, morphology and crystallinity. Properties and characterization of nanocellulose and nanocellulose-based composites: Elsevier; 2026. p. 1-39.

21. Yodsanga S, Poeaim S, Chantarangsu S, Swasdison S. Investigation of biodegradation and biocompatibility of chitosan–bacterial cellulose composite scaffold for bone tissue engineering applications. Cells 2025;14(10):723 .

22. Shen T, Dong H, Wang P. Research progress on nanocellulose and its composite materials as orthopedic implant biomaterials. Alex. Eng. J. 2024;87:575-90 .

23. Wang H ,Cao L, Wang X, Lang X, Cong W, Han L, et al. Effects of isocyanate structure on the properties of polyurethane: Synthesis, performance and self-healing characteristics. Polym. 2024;16(21):3045 .

24. Kucinska-Lipka J, Gubanska I, Janik H, Sienkiewicz M. Fabrication of polyurethane and polyurethane based composite fibres by the electrospinning technique for soft tissue engineering of cardiovascular system. Mater. Sci. Eng. C 2015;46:166-76 .

25. Szczepańczyk P, Szlachta M, Złocista-Szewczyk N, Chłopek J, Pielichowska K. Recent developments in polyurethane-based materials for bone tissue engineering. Polym. 2021;13(6):946 .

26. Prasadh S, Suresh S, Wong R. Osteogenic potential of graphene in bone tissue engineering scaffolds. Mater. 2018;11(8):1430 .

27. Bakshi A, Bustamante H, Sui X, Joshi R. Structure dependent water transport in membranes based on two-dimensional materials. Ind. Eng. Chem. Res. 2021;60(30):10917-59 .

28. Dubey N, Bentini R, Islam I, Cao T ,Castro Neto AH, Rosa V. Graphene: A versatile carbon-based material for bone tissue engineering. Stem Cells Int. 2015;2015 .

29. Wang T, Zhang M, Guo J, Wei H, Li W, Luo Y. Alginate/bacterial cellulose/gelma scaffolds with aligned nanopatterns and hollow channel networks for vascularized bone repair. Int. J. Biol. Macromol. 2025;308:142578 .

30. Jin S, Wen J, Zhang Y, Mou P, Luo Z, Cai Y, et al. M2 macrophage-derived exosome-functionalized topological scaffolds regulate the foreign body response and the coupling of angio/osteoclasto/osteogenesis. Acta Biomater. 2024;177:91-106 .

31. Wang S-J, Deng R-H, Song C-H, Yuan F-Z, Li P-Q, Cao X-Y, et al. Biomechanically matched and multistage hybrid porous scaffolds for stem cell-based osteochondral regeneration. Nano Today 2024;59:102539 .

32. Kontogianni G-I, Loukelis K, Bonatti AF, Batoni E, De Maria C, Vozzi G, et al. A mechanically stimulated co-culture in 3-dimensional composite scaffolds promotes osteogenic and anti-osteoclastogenic activity and m2 macrophage polarization. Biomater. Res. 2025;29:0135 .

33. Wu H, Zhong X, Leng P, Sun C, Xie B, Liu L, et al. 3d-printed oxygen-releasing scaffolds promote bone repair via angiogenesis and osteogenesis. APL Mater. 2025;13 .(١٢)

34. Mahmoudifard M, Soleimani M, Hatamie S, Zamanlui S, Ranjbarvan P, Vossoughi M, et al. The different fate of satellite cells on conductive composite electrospun nanofibers with graphene and graphene oxide nanosheets. Biomed. Mater. 2016;11 ٠٢٥٠٠٦:(٢)

35. Janmohammadi M, Nazemi Z, Salehi AOM, Seyfoori A, John JV, Nourbakhsh MS, et al. Cellulose-based composite scaffolds for bone tissue engineering and localized drug delivery. Bioact. Mater. 2023;20:137-63 .

36. Khoramgah MS, Ranjbari J, Abbaszadeh H-A, Mirakabad FST, Hatami S, Hosseinzadeh S, et al. Freeze-dried multiscale porous nanofibrous three dimensional scaffolds for bone regenerations. BI. 2020;10(2):73 .

37. Azari A, Rahimi A, Rajabibazl M, Abbaszadeh HA, Hosseinzadeh S, Rahimpour A. Evaluation of in vitro coculture of keratinocytes derived from foreskin and adipose-derived mesenchymal stem cells (amscs) on a multilayer oxygen-releasing electrospun scaffold based on pu/pcl. Sodium percarbonate (spc)-gelatine/pu. Cell Biochem. Funct. 2023;41(4):434-49 .

38. Shahghasempour L, Fattahi R, Hosseinzadeh S, Haddadi A, Shams F. In vivo assessment of lactobacillus plantarum and co-cultured cells on a polyurethane/prgf/gelatin/polyurethane scaffold in skin wound healing. SPE Polym. 2024;5(4):637-62 .

39. Azizi M, Navidbakhsh M, Hosseinzadeh S, Sajjadi M. Cardiac cell differentiation of muscle satellite cells on aligned composite electrospun polyurethane with reduced graphene oxide. J. Polym. Res. 2019;26(11):1-9 .
40. Banihashemian SA, Benisi SZ, Hosseinzadeh S, Shojaei S, Abbaszadeh HA. Chitosan/hyaluronan and alginate-nanohydroxyapatite biphasic scaffold as a promising matrix for osteoarthritis disorders. Adv. Pharm. Bull. 2024;14(1):176 .
41. Unnithan AR, Park CH, Kim CS. Nanoengineered bioactive 3d composite scaffold: A unique combination of graphene oxide and nanotopography for tissue engineering applications. Compos. B: Eng. 2016;90:503-11 .
42. Kashte SB, Kadam S, Maffulli N, Potty AG, Migliorini F, Gupta A. Osteoinductive potential of graphene and graphene oxide for bone tissue engineering: A comparative study. J. orthop. surg. res. 2024;19(1):527 .
43. Ansari S, Ito K, Hofmann S. Alkaline phosphatase activity of serum affects osteogenic differentiation cultures. ACS Omega 2022;7(15):12724-33 .
44. Deng Y, Zhu T, Cheng Y, Zhao K, Meng Z, Huang J, et al. Recent advances in functional cellulose-based materials: Classification, properties and applications. Adv. Fiber Mater. 2024;6(5):1343-68 .
45. Othman HS, Elsayed AE, Nawwar G. Microcrystalline cellulose acetate incorporating cyanoacetyl moiety. Biomass Convers. Biorefin. 2025;15(9):14199-210 .
46. Abd El-Aziz FE-ZA, Hetta HF, Abd Ellah NH, Abd El-Aal M. Antibacterial and healing potential of zn-al ldhs/cellulose acetate nanocomposite in burns and wounds: A study on earthworms as a human skin model. J. Inorg. Organomet. Polym. Mater. 2025;35(3):1615-26 .
47. Kalita NK, Hakkarainen M. Triggering degradation of cellulose acetate by embedded enzymes: Accelerated enzymatic degradation and biodegradation under simulated composting conditions. Biomacromolecules 2023;24(7):3290-303 .
48. Zhijiang C, Yi X, Haizheng Y, Jia J, Liu Y. Poly (hydroxybutyrate)/cellulose acetate blend nanofiber scaffolds: Preparation, characterization and cytocompatibility. Mater. Sci. Eng. C 2016;58:757-67 .
49. Dolati S, Sadreddini S, Rostamzadeh D, Ahmadi M, Jadidi-Niaragh F, Yousefi M. Utilization of nanoparticle technology in rheumatoid arthritis treatment. Biomed. pharmacother. 2016;80:30-41 .
50. Vickers NJ. Animal communication: When i’m calling you, will you answer too? Curr. Biol. 2017;27(14):R713-R5 .
51. Shams F, Moravvej H, Hosseinzadeh S, Mostafavi E, Bayat H, Kazemi B, et al. Overexpression of vegf in dermal fibroblast cells accelerates the angiogenesis and wound healing function: In vitro and in vivo studies. Sci. Rep. 2022;12(1):18529. doi: 10.1038/s41598-022-23304-8

52. Aidun A, Safaei Firoozabady A, Moharrami M, Ahmadi A, Haghighipour N, Bonakdar S, et al. Graphene oxide incorporated polycaprolactone/chitosan/collagen electrospun scaffold: Enhanced osteogenic properties for bone tissue engineering. Artif. Organs 2019;43(10):E264-E81 .
53. Yang J, Li R, Wang X, Lu D, Li W ,Wang Y. Mechanically tunable fiber-based hydrogel activates piezo1–integrin axis for enhanced bone repair. J. Nanobiotechnology 2025;23(1):603 .
54. Qin Y, Jing Z, Zou D, Wang Y, Yang H, Chen K, et al. A metamaterial scaffold beyond modulus limits: Enhanced osteogenesis and angiogenesis of critical bone defects. Nat. Commun. 2025;16(1):2180 .
55. Fu C, Bai H, Hu Q, Gao T, Bai Y. Enhanced proliferation and osteogenic differentiation of mc3t3-e1 pre-osteoblasts on graphene oxide-impregnated plga–gelatin nanocomposite fibrous membranes. RSC Adv. 2017;7(15):8886-97 .
56. Esmaeili E, Eslami-Arshaghi T, Hosseinzadeh S, Elahirad E, Jamalpoor Z, Hatamie S, et al. The biomedical potential of cellulose acetate/polyurethane nanofibrous mats containing reduced graphene oxide/silver nanocomposites and curcumin: Antimicrobial performance and cutaneous wound healing. Int. J. Biol. Macromol. 2020;152:418-27 .
57. Shams F, Moravvej H, Hosseinzadeh S, Kazemi B, Rajabibazl M ,Rahimpour A. Evaluation of in vitro fibroblast migration by electrospun triple-layered pu-ca/gelatin. Prgf/pu-ca scaffold using an aavs1 targeted egfp reporter cell line. BI 2021;12(3):219 .
58. Staji M, Sadeghzadeh N, Zamanlui S, Azarani M ,Golchin A, Soleimani M, et al. Evaluation of dermal growth of keratinocytes derived from foreskin in co-culture condition with mesenchymal stem cells on polyurethane/gelatin/amnion scaffold. Int. J. Polym. Mater. Polym. Biomater. 2021:1-11 .
59. Elkhenany H, Amelse L, Lafont A, Bourdo S, Caldwell M, Neilsen N, et al. Graphene supports in vitro proliferation and osteogenic differentiation of goat adult mesenchymal stem cells: Potential for bone tissue engineering. J. Appl. Toxicol. 2015;35(4):367-74 .
60. Sun M, Chi G, Li P, Lv S, Xu J, Xu Z, et al. Effects of matrix stiffness on the morphology, adhesion, proliferation and osteogenic differentiation of mesenchymal stem cells. Int. J. Med. Sci. 2018;15(3):257 .

Table 1. A summary of running clinical studies related to applications of MSCs.

No.	Cell source	Approaches	Results	ID of clinicaltrials.gov-last updated
1	AMSCs, BM-MSCs and UC-MSCs	Bone defects	Better formation of non - union bone fracture with BM-MSCs	NCT02307435-2014
2	BM-MSCs	Osteonecrosis	Lower pain and bone formation	NCT02566681-2017
3	BM-MSCs	Bone defects	new bone tissue with lower time	NCT03103295-2017
4	BM-MSCs	Amyotrophic Lateral Sclerosis	High safety and better respiratory function	NCT01051882-2019
5	BM-MSCs	Spinal Cord Injury	axonal regeneration and functional recovery	NCT02981576-2019
6	BM-MSCs	Spinal fusion	The cells were safe and the fusion was a challenge	NCT01552707-2020
7	BM-MSCs	Jaw bone	Restoration of mandibular	NCT02751125-2020
8	BM-MSCs	Jaw bone	Augmentation of the alveolar ridge	NCT04297813-2020
9	BM-MSCs	Degenerative Disc Disease	Low pain and tissue improvement	NCT04499105-2020
10	BM-MSCs	Osteoporosis	Lower pain and better functionality	NCT02566655-2020
11	BM-MSCs	osteoarthritis	Safety, low pain and functional improvement	NCT04240873-2020
12	BM-MSCs	Chronic LBP	pain relief	NCT05066334-2021
13	BM-MSCs	Bone defects	Formation of callus	NCT01429012-2021
14	BM-MSCs	Knee osteoarthritis	Lower pain, better function	NCT03589287-2021

			and higher cartilage thickness of knee	
15	BM-MSCs	Multiple sclerosis	activated cells of MSCs and high proliferation of lymphocytes	NCT00781872 -2021
16	BM-MSCs	Long bone fractures	Bone formation around fracture ends	NCT04340284-2022
17	BM-MSCs	Long bone fractures	Bone healing	NCT03325504-2022
18	BM-MSCs	Bone defects	Formation of dental root and a full-thickness flap	NCT05975892-2023
19	AMSCs	Enhancer of bone formation	Bone formation	NCT04998058-2024
20	BM-MSCs	Multiple sclerosis	Better muscle strength and bladder function	NCT03355365-2024
21	UC-MSC	Osteonecrosis	core decompression of bone	NCT03180463-2024

Table 2. Mechanical tensile properties of PU, PU-CA and PU-CA-GO scaffolds.

Scaffolds\ Property	**Strain (%)**	**Ultimate tensile strength (MPa)**	**Young modulus (MPa)**
PU	230	3.68	1.024
PU-CA	8.54	4.87	1.29
PU-CA-GO	9.37	5.98	1.38

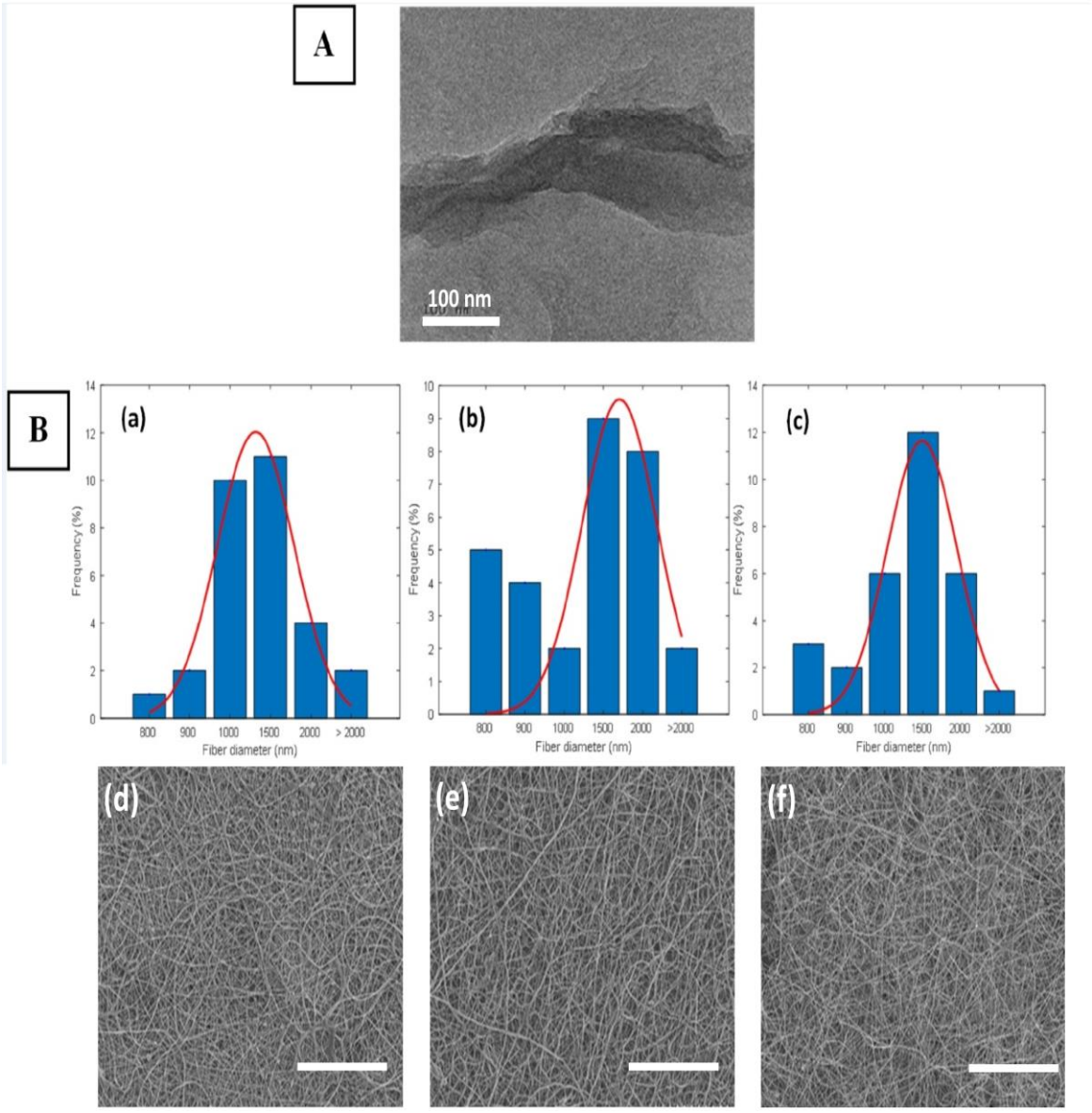

Figure 1. (A) Investigation of synthesized GO nanoparticles by TEM, (B) Fiber diameter distribution and morphology of PU (a, d), PU-CA (b, e) and PU-CA –GO (c, f) scaffolds. The scale bar is 100 µm.

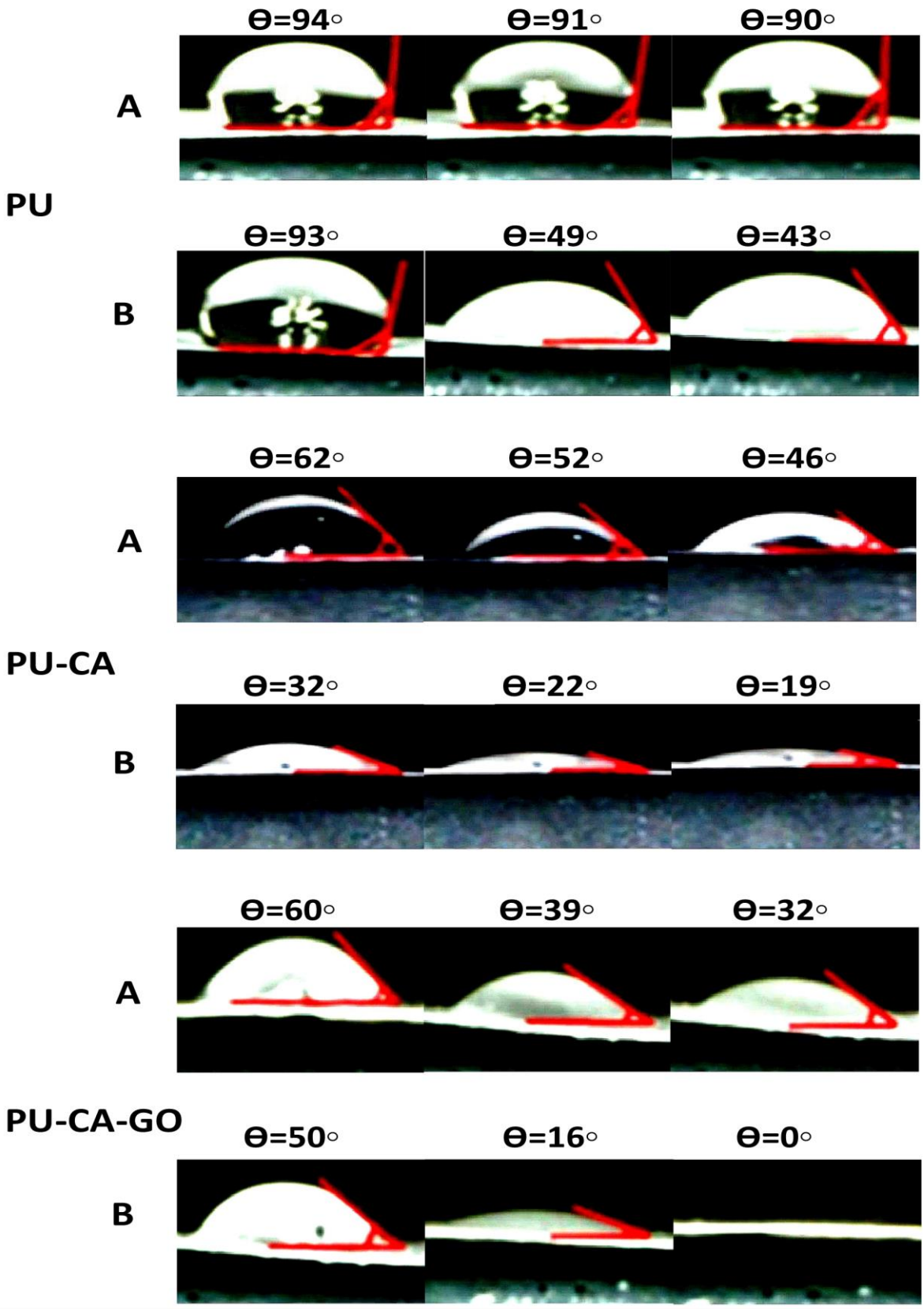

Figure 2. Contact angle quantification of PU, PU-CA and PU-CA-GO scaffolds before plasma treatment (A) and after plasma treatment (B).

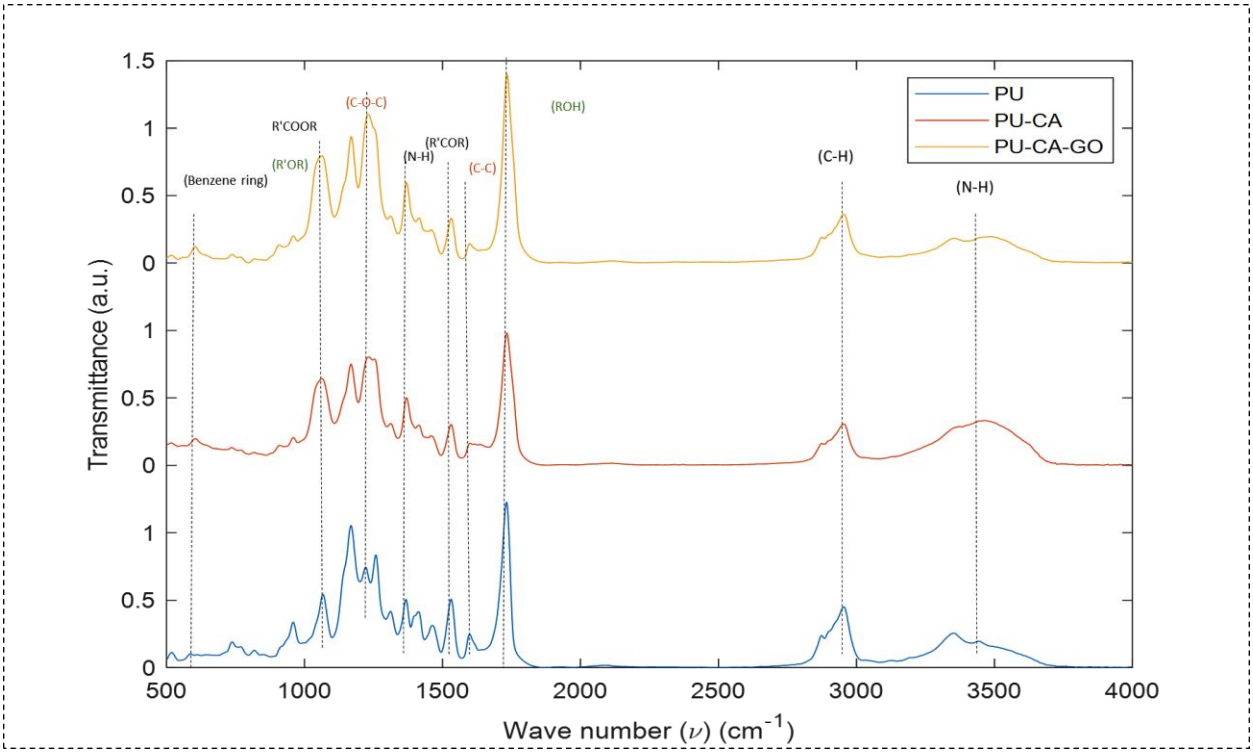

Figure 3. FTIR spectra of PU (blue line), PU-CA (red line) and PU-CA-GO (orange line) scaffolds. Black functional groups (PU peaks), Green functional groups (CA peaks) and Orange functional groups (GO peaks).

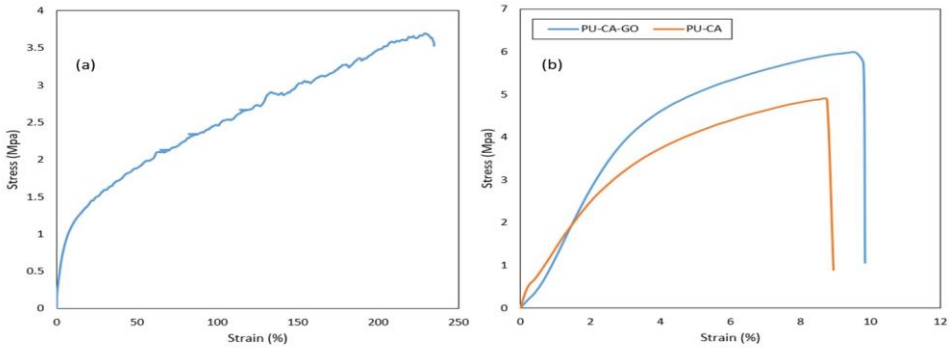

Figure 4. (a) Representative stress-strain curves of PU, (b) PU-CA (red line) and PU-CA-GO (blue line).

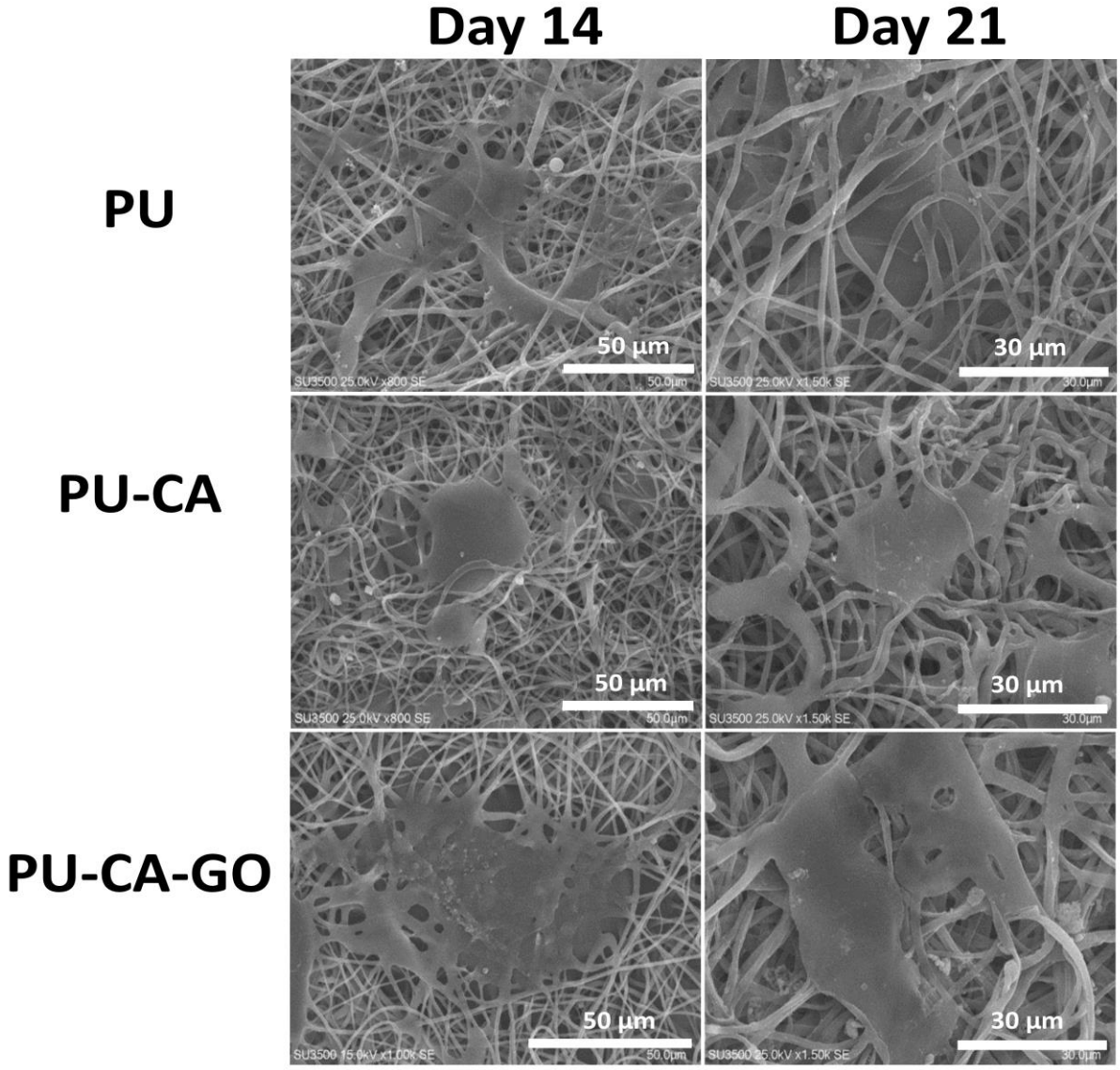

Figure 5. Cellular morphology by SEM on PU, PU-CA and PU-CA-GO scaffolds after 14 and 21 days.

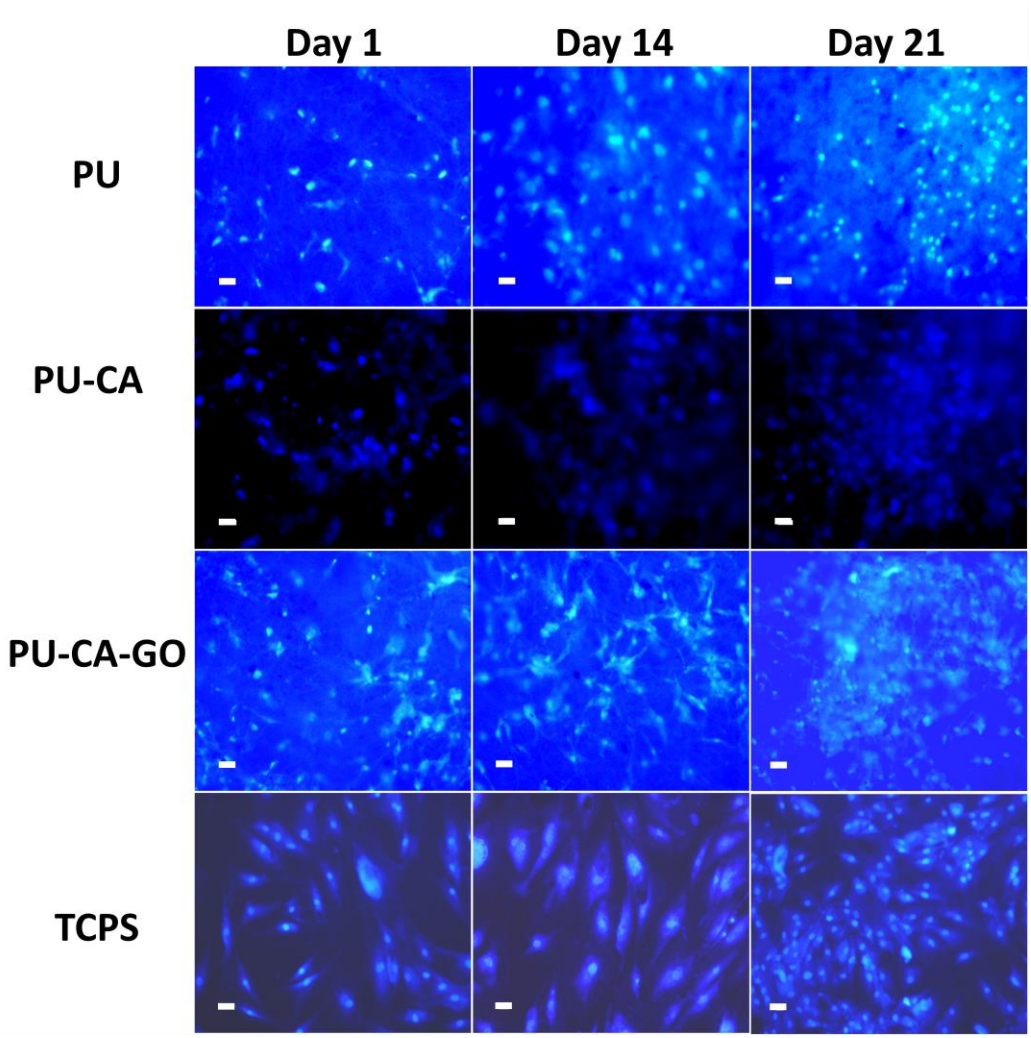

Figure 6. Cell presence on PU, PU-CA and PU-CA-GO scaffolds and TCPS through DAPI staining. The scale bar is 10 µm.

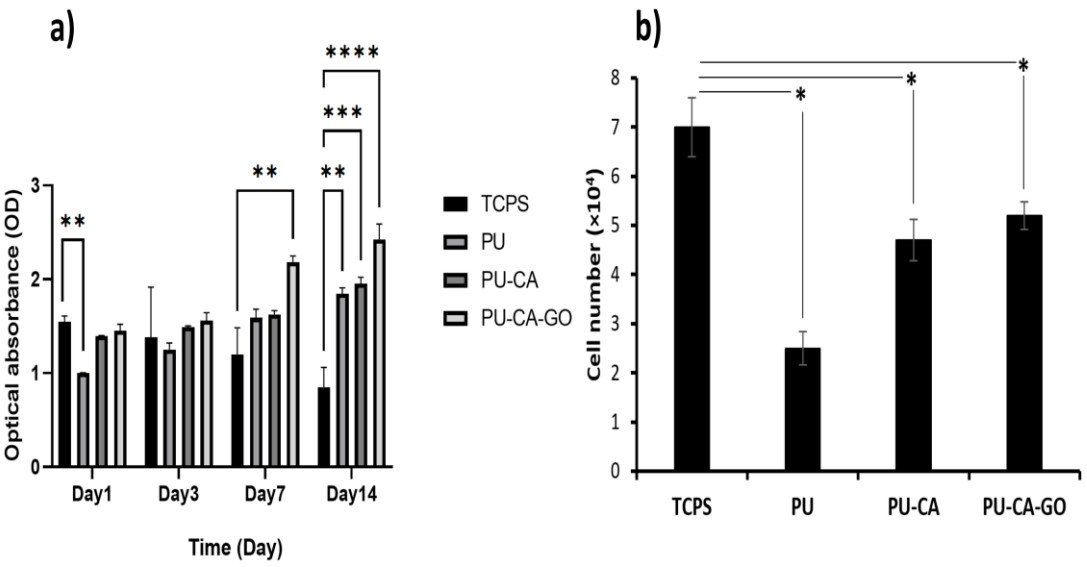

Figure 7. (a) Cell viability of MSCs on TCPS and the scaffolds after 1, 3, 7 and 14 days (****P ≤ 0.001, ***P ≤ 0.01, ** P ≤ 0.05) and (b) Cell numbers after 4 hours of MSCs seeding on TCPS and the scaffold groups.

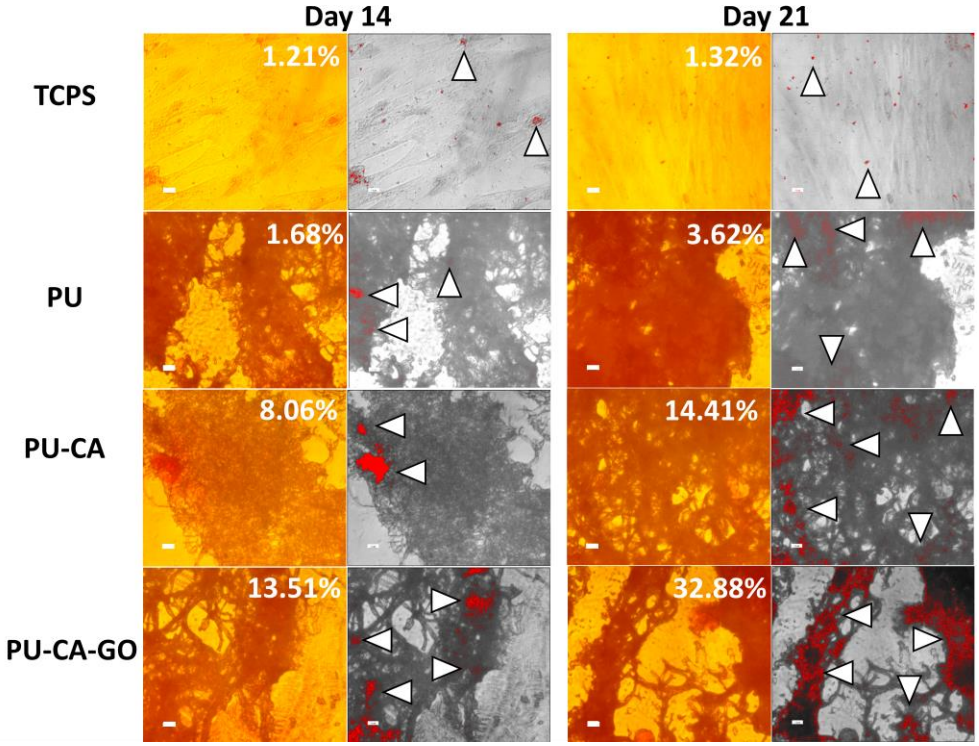

Figure 8. Alizarin Red staining of TCPS, PU, PU-CA and PU-CA-GO groups and their analysis by ImageJ software. The scale bar is 10 µm and the arrows present the mineralized regions.

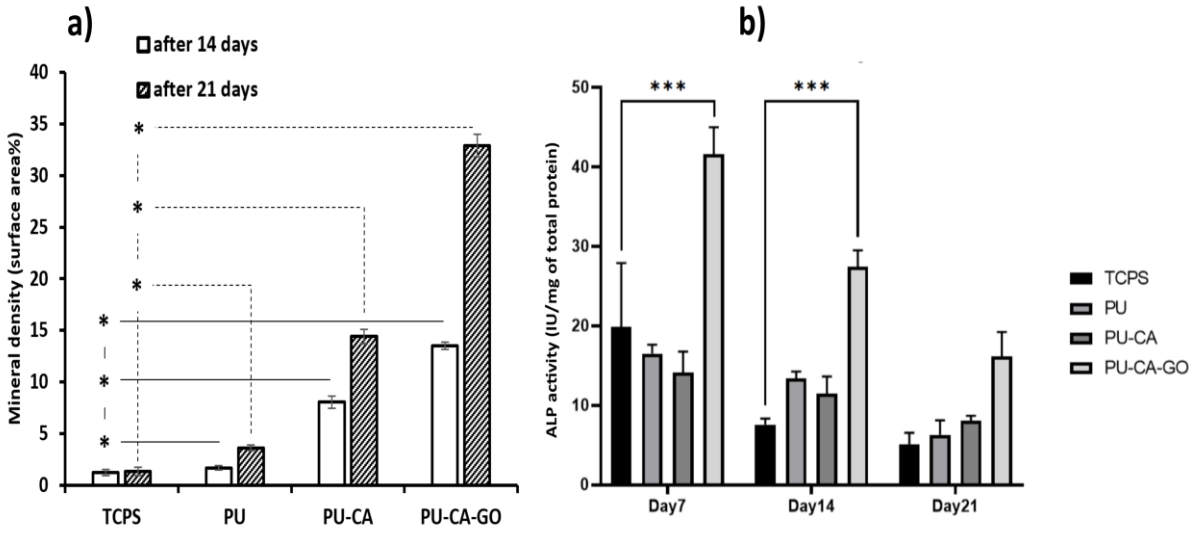

Figure 9. (a) Mineral density of TCPS, PU, PU-CA and PU-CA-GO groups and (b) ALP activity of MSCs on TCPS, PU, PU-CA and PU-CA-GO scaffolds and TCPS at days 7,14 and 21 (*** $P \leq 0.01$).

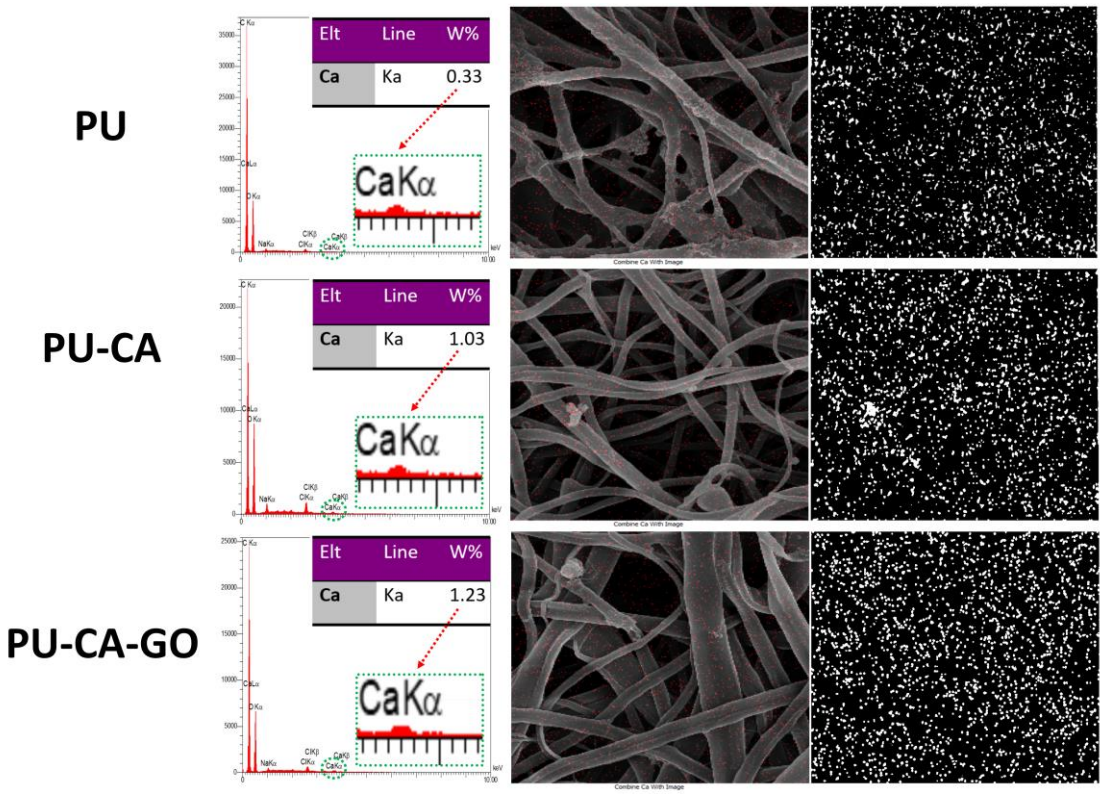

Figure 10. EDS analysis for calcium content after culture of MSCs on PU, PU-CA and PU-CA-GO scaffolds for 21 days. The arrows present the band of Kα originated from calcium.

Supplementary file 1. The characterization of MSCs derived from adipose tissue by flow cytometry.